# A modelling study of the flow pattern in a rotating drum for aerosol aging

Emma M. M. Wingstedt, Kristin Pedersen and Bjørn Anders P. Reif

Norwegian Defence Research Establishment (FFI)

19 November 2009

FFI-rapport 2009/01079

1112

P: ISBN 978-82-464-1670-0
E: ISBN 978-82-464-1671-7

## Keywords

Aerosoler

CFD

Roterende kammer

## Approved by

| | |
|---|---|
| Bjørn Anders Pettersson Reif | Project Manager |
| Jan Ivar Botnan | Director |

# English summary

Aerosols are small droplets or particles suspended in a gas and they can contain microorganisms or other harmful substances. It is therefore of great importance to gain more knowledge about them, for example their survival time and how they disperse. For best control of the factors affecting the aerosols, studies are best performed in an aerosol chamber. Today, almost all aerosol chambers in use are stationary and maintained by stirred settling of aerosols. However, literatures suggest that it would be possible to keep particles airborne for a significantly longer period of time if the chamber was rotating. A schematic of such a rotating aerosol chamber is shown in figure 0.1.

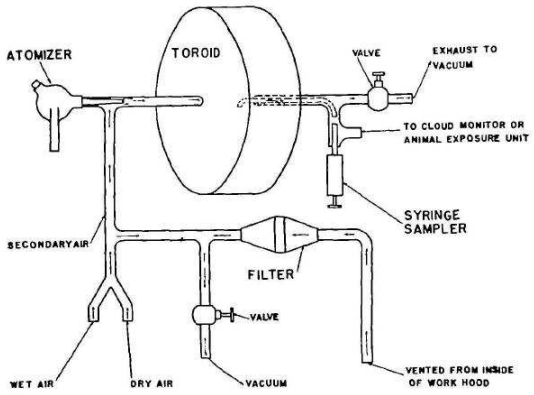


*Figure 0.1 Simplified schematic air flow diagram of toroid installation (1)*

In this study the flow within a rotating aerosol chamber was modelled using CFD. The primary objective was to study the aerosol tracks inside the chamber in order to understand the very long residence times observed in full scale laboratory experiments. This has not been discussed in any of the most well known literature on the topic although it constitutes the key to understand this phenomenon. A secondary objective was to use a number of different turbulence models in order to investigate their significance for the predicted results.

When aerosols were injected in the centre of the chamber along the axis of rotation, the simulations showed that they would very slowly be transported axially towards the circular sidewall of the chamber. If the injection took place off the axis of rotation, the aerosols would at the same time rotate in the tangential direction. As the aerosols approach the sidewall, they would be further displaces from the axis of rotation and rotate in larger and larger tangential circles which transport them radially towards the peripheral outer wall. When the outer wall is approached, the aerosols would be transported back towards the symmetry plane of the chamber and then back towards the centre of the chamber in a spiralling motion. A rough estimate of the residence time gives that the time it takes for a particle to circulate the chamber once is in order of hours - and furthermore that the aerosols that are not deposited on the chamber walls can be kept in the air for many hours, even in the order of days. The present results thus seem fully consistent with the experimental findings. This confirms that the CFD approach can be used to conduct detailed studies of aerosol transport in rotating chambers and as such be a valuable addition to full scale experiments.

The result also showed a substantially difference between the results given by the different models, some of which seem physically unrealistic. The lesson learned is that great care has to be taken about which specific approach that should be adopted.

# Sammendrag

Aerosoler er små dråper eller partikler som kan transporteres med i luft. Disse kan inneholde mikroorganismer eller andre farlige substanser. Det er derfor viktig å studere aerosoler for å få kjennskap til de parametre som bestemmer deres overlevingstid. For å ha best mulig kontroll over de faktorer som påvirker aerosolene gjennomføres ofte undersøkelser under kontrollerte forhold inne i spesielt konstruerte aerosolkamre. Nesten alle aerosolkamre som anvendes i dag er stasjonære der aerosolene holdes i luften gjennom at luften blir rørt om. Dog hevdes det i litteraturen at det ville være mulig å holde partikler i luften en mye lengre periode dersom kammeret roterer, se figure 0.1.

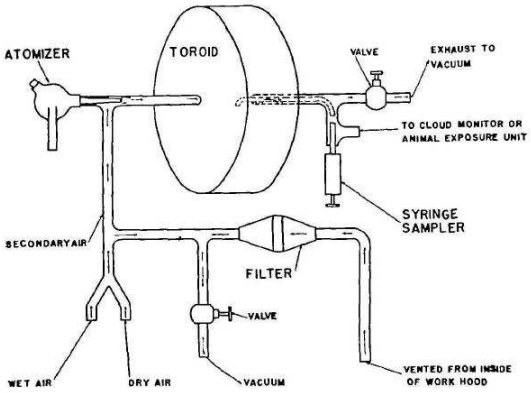


*Figure 0.1 Simplified schematic air flow diagram of toroid installation (1)*

I denne studien er strømningen i et roterende aerosolkammer modellert med CFD. Hovedmotivasjonen for studien er å bestemme partikkelbanene til aerosolene i kammeret for å søke å forstå hvordan aerosolene kan holdes i luften under svært lange tidsperioder (mer enn i et døgn) i et slikt kammer. Et sekundært formål med studien har vært å bruke forskjellige turbulensmodeller for å øke forståelsen av hvor viktige disse er.

Simuleringene viser at hvis aerosoler blir injisert midt i kammeret langs rotasjonsaksen så vil disse først bevege seg sakte aksialt mot den sirkulære sideveggen. Hvis aerosolene blir injisert et lite stykke unna rotasjonsaksen, så vil disse samtidig rotere i tangential retning. Når aerosolene nærmer seg den sirkulære sideveggen, vil de bli transport radielt og derved også rotere i større og større baner. Aerosolene vil følgelig langsomt bli transport radielt mot den ytre veggen. Når de nærme seg den ytre veggen, beveger aerosolene seg inn mot symmetriplanet igjen og deretter tilbake mot midten av kammeret i en spiralformet bevegelse. En grov overslagsberegning viser at tiden det tar for en partikkel å sirkulere kammeret en gang er av størrelsesorden timer. Hvis deposisjonsraten av aerosolene på kammerets vegger er liten vil aerosolene kunne holdes i luften en veldig lang tid - opp mot dager. Resultatene viser og at det vil skje en agglomerering av aerosoler langs den ytre veggen av kamret. CFD-beregninger ser altså ut å være i stand til å reprodusere hva som er blitt eksperimentelt observert og denne studien viser da samtidig at CFD kan vare et verdifullt komplimenterende verktøy til fullskala aerosol eksperimenter for å øke forståelsen av transportprosessen.

Studien viser også til dels store forskjeller mellom resultatene fra de ulike turbulensmodellerne, og at noen av disse resulterer i en ufysikalsk oppførsel. Riktig bruk av CFD krever derfor god strømningsfysikalsk innsikt for å være i stand til å velge egnet metodikk.

# Contents

# 1 Introduction

This work was partly conducted by the second author during a summer internship at FFI and is an introductory study of aerosol transport in aerosol chambers.

Aerosols are small droplets or particles suspended in a gas, which can contain microorganisms or substances harmful to both the environment and animal and human life. Just imagine phenomena such as pollution or deceases caused by inhalation of asbestos fibers. Sneezing whilst having a flu creates aerosols containing the virus, which in turn transmits the decease to other people. The use of biological weapons springs to mind, as well as other deceases which also spread the same way. In the mid-14th century, the black plague wiped out approximately 3/4 of Europe's population, forever changing the course of history of this region. To prevent such a disaster from happening again, our knowledge of aerosols and microorganisms in general must be improved, and in particular we wish to predict the paths of the aerosols and the survival time of the microorganisms within.

For best control of the factors affecting the organisms, such as air temperature and relative humidity, studies conducted on aerosols are best performed in an aerosol chamber. Such chambers were traditionally stationary, and maintained by stirred settling of aerosols. However, many properties of aerosols are functions of time and the study of these characteristics therefore require aging of the aerosols. In the traditional chambers, physical loss due to gravitational settling limits the survival time. The height of the chamber will in this case determine the aerosol holding time (1), and to prolong the study a taller chamber has to be built. Needless to say, this approach has both financial and practical limits.

The use of rotating chambers for aerosol aging was first suggested in 1958 by Goldberg et al. (2). The rotational movement of the drum will cause the particles to remain airborne for a substantially longer period of time, compared to the simple stirred settling chambers. Goldberg et. al. managed to keep particles of 1 to 2 $\mu m$ airborne for 2 days with the physical loss not exceeding 50 percent.

In this short study, the flow within the rotating chamber is modelled using computational fluid dynamics (CFD), to determine the particle tracks aerosols would follow if injected into the center. Assuming the aerosols can be considered as passive scalars, they will not influence the flow itself, and the modelling of the flow will indeed predict the paths of the particles. This assumption holds for aerosols of similar physical properties as the medium which contains them, in this case air.

The CFD software used to model the flow was Fluent. Another important objective in this study is to compare the different turbulence models that Fluent provides.

### 1.1 The aerosol chamber

The chamber consists of an air-filled drum, 0.6096 meters (2 feet) wide and 1.8288 meters (6 feet) in diameter, that is free to rotate around the axis of symmetry, and does so at a constant rotational speed of 5 rpm. The drum is illustrated in figure 1.1. The axis of symmetry is the z-axis, and from this angle of view, the drum is rotating counterclockwise.

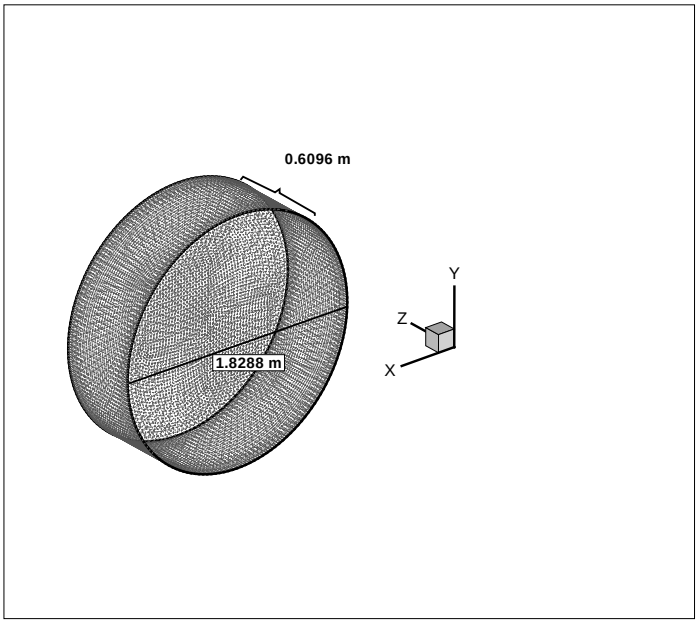


*Figure 1.1 Rotating drum and computational grid.*

## 2 Governing equations

NOMENCLATURE

$T_{ij}^{(v)}$ - viscous shear stress tensor

$\rho$ - density

$p$ - static pressure

$f_i$ - external forces

$u_i$ - fluid velocity, i-th component

$\vec{\omega}$ - angular velocity

$\vec{v}$ - absolute velocity vector

$\vec{v_r}$ - relative velocity vector

The equations describing the fluid motion within the drum are the Navier-Stokes (N-S) equations. Derived from the conservation laws of mass and momentum, they are given by

$$\rho(\frac{\partial u_i}{\partial t} + u_j \frac{\partial u_i}{\partial x_j}) = -\frac{\partial p}{\partial x_i} + \frac{\partial T_{ij}^{(v)}}{\partial x_j} + f_i \tag{2.1}$$

$$\frac{\partial \rho}{\partial t} + \frac{\partial \rho u_i}{\partial x_i} = 0 \tag{2.2}$$

Here, $u_i = u_i(\vec{x}, t)$ is the i-th component of the fluid velocity at a point $\vec{x}$ in space and at time t. Einstein summation convention applies, giving summation over repeated indices; e.g.

$$\frac{\partial u_j}{\partial x_j} = \frac{\partial u_1}{\partial x_1} + \frac{\partial u_2}{\partial x_2} + \frac{\partial u_3}{\partial x_3}$$

as the subscript $i$ can take on the values 1, 2 or 3. For an incompressible fluid, $\frac{D\rho}{Dt} = 0$, and so 2.2 is reduced to

$$\frac{\partial u_i}{\partial x_i} = 0 \tag{2.3}$$

## 2.1 RANS equations and turbulence models

In general an analytic solution to Navier-Stokes equations cannot be found, and we need to find numerical approximations to the solutions. Turbulence contains different scales of motion, often called eddies, and the large eddies will transfer their energy to the smaller ones through the energy cascade. At the smallest scales the energy dissipates to heat. To avoid directly simulating the small scale fluctuations, we can use Reynold-averaging or filtering of the N-S equations.

In a large eddy simulation (LES), which has its basis in the filtered approach, large eddies are computed in a time-dependent and always three-dimensional simulation, while the small eddies are modelled. It is argued that this will reduce the error introduced by turbulence modelling, as less of the turbulence actually is modelled. Large eddies will be more subdued by the geometries of the CFD domain, whereas the small eddies are assumed to be nearly isotropic, i.e., directionally independent, and so a model for the small scale eddies will emerge more easily. The LES uses a filtered form of the N-S equations, which has the smallest eddies removed, typically of the order of the grid size. This filtering process also induces additional terms that must be modelled.

In the RANS models, the solution variables in the exact N-S are decomposed into mean (ensemble-averaged) and fluctuating components, and so the average of all turbulence scales are modelled. For instance, the instantaneous velocity components will be given as

$$u_i(x, y, z, t) = \bar{u_i}(x, y, z, t) + u_i'(x, y, z, t)$$

where $\bar{u_i}$ is the averaged part and $u_i'$ is the fluctuating part. Other scalar components will be given in a similar way. Substituting this into the N-S equations, and taking the average, we get the ensemble-averaged momentum equation:

$$\rho(\frac{\partial \bar{u_i}}{\partial t} + \bar{u_i}\frac{\partial \bar{u_i}}{\partial x_j}) = -\frac{\partial \bar{p}}{\partial x_i} + \frac{\partial}{\partial x_j}(T_{ij}^{(v)} - \rho\overline{u_i'u_j'}) + \bar{f}_i \tag{2.4}$$

The averaged form of equation 2.3 and equation 2.4 are known as the Reynolds-averaged Navier-Stokes (RANS) equations, which are the ones modelled in the RANS models. The terms $-\overline{u_i'u_j'}$ are the Reynolds stresses, which need to be modelled as well, and this term is treated differently in the different models. The reader is referred to the Fluent user's guide (3) for more details on available models in Fluent.

Several models based on the Reynolds Averaged Navier-Stokes equations are compared in this study, as well as a laminar model and a Large Eddy Simulation.

## 2.2 Equations in a rotating frame of reference

In modelling of this problem, the use of a rotating frame of reference will prove to be advantageous. The equations of motion will then be modified to incorporate additional acceleration terms due to the transformation from a stationary to a moving reference frame. The symmetry and simplicity of the drum makes it possible to view the entire domain in a single frame of reference, and so the walls can be considered at rest relative to the rotating interior. This make steady-state solutions possible even though the problem could be unsteady in the stationary frame, so long as the rotational speed is constant.

Assume our coordinate system containing the CFD domain is rotating with a constant angular velocity $\vec{\omega}$ relative to the stationary reference frame, and that a point in the CFD domain is located at $\vec{r}$. The fluid velocities are transformed from the stationary frame to the rotational frame by:

$$\vec{v_r} = \vec{v} - \vec{u_r}$$

where

$$\vec{u_r} = \vec{\omega} \times \vec{r}$$

Here, $\vec{v}_r$ and $\vec{v}$ are the relative and absolute velocities, respectively, and $\vec{u}_r$ is the swirl velocity due to the rotating frame. This conversion will affect the N-S equations, which in turn affects the RANS equations. Details on the resulting equations can be found in the Fluent User's guide (3).

# 3 Simulations

The preprocessor for Fluent has in this study been Gambit. As the models have different requirement to the grids on which they are applied, three different grids were constructed to reduce computational time. For instance, the $k-\varepsilon$ models were applied to a relatively coarse grid of 112 000 cells whereas the $k-\omega$ models were applied to a grid of approximately 1 000 000 cells. Requiring a very fine, uniform grid the LES, as well as the laminar model, was applied to a grid of 5 000 000 cells. All grids used the so-called map meshing scheme.

The rotational speed was set to 5 rpm (or, equivalently, $\frac{\pi}{6}$ rad/s) of the moving reference frame. The walls were set as stationary relative to this. In the corresponding stationary reference frame, the walls then has a tangential velocity of 0.479 m/s. The drum was set to be filled with air, and a no-slip condition specified on all walls. The pressure based solver has been used, with first-order upwind discretization schemes. For pressure, the scheme PRESTO! has been applied, as this is recommended in the Fluent manual for rotating domains. For all methods, enhanced wall treatment has been used.

The models were run until the wall speed and the wall shear stress of the periphery became constant. As there are no parameters besides the wall speed to which we know the analytical answer, these became the convergence criterions. Some models were fairly reluctant to converge, including the laminar model and the $k-\varepsilon$ model with non-equilibrium wall functions. The reason the models take so long to converge is probably the low velocities compared to the large drum. This means the solution variable changes little between time-steps. Some models, such as the $k-\varepsilon$ standard, did converge according to the criterions, but looking at the finalized contour plots, they were not entirely symmetric.

# 4 Results

## 4.1 The flow pattern and particle paths

In this section, the general flow pattern will be described. The $k-\varepsilon$ RNG model will be considered, as this gives the most reliable result (cf. section 4.2). The figure 4.1 shows the streamlines of velocity in the plane y = 0. A particle inserted somewhere in the inner region will follow these streamlines, as long as the physical properties of the particle are similar to those of air. This is true for very small particles. Also shown are contours of tangential velocity, or y-velocity. As the y-axis here points into the plane, y-velocity is the velocity into or out of the plane, hence being normal to the plotted streamlines. A positive y-velocity (red color) means flow into the plane, and negative (blue color) means flow out of the plane. The maximum value of tangential velocity is 0.47 m/s, which is the velocity of the walls and thereby consistent of our rotational speed of 5 rpm. The value decreases rapidly near the wall and is close to zero in most of the middle region. This makes sense as it is closer to the rotational axis (z).

We can recognize the same pattern in figure 4.2, showing the actual tangential velocity in the plane z = 0.25. This has the same scale, except it has no negative part as nothing rotates the other way. More interesting are the contours of axial velocity, shown in figure 4.3. Axial velocity is the velocity in the z-direction. Being mostly red, most of the interior is moving in positive z-direction (out of the paper), but closer to the wall, the direction shifts to negative z-direction. This is consistent with the streamlines in figure 4.1. Had we plotted contours in a plane of constant negative value, say z = -0.25, they would look inverted.

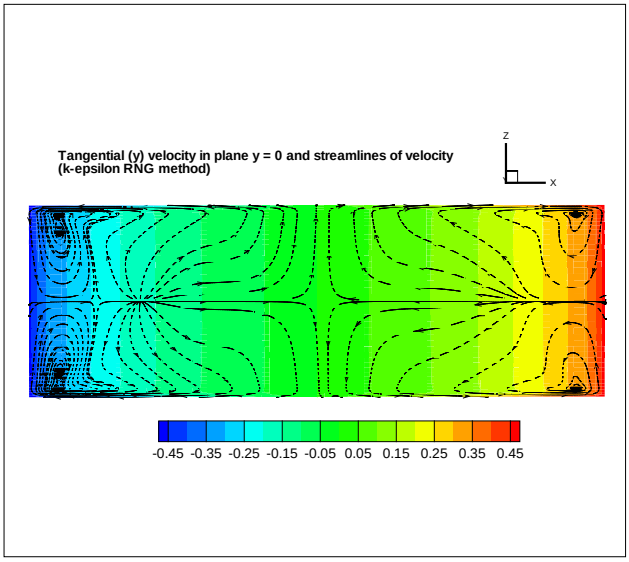


*Figure 4.1 Tangential (y) velocity and streamlines of velocity in the plane y = 0. (cf. fig. 4.8)*

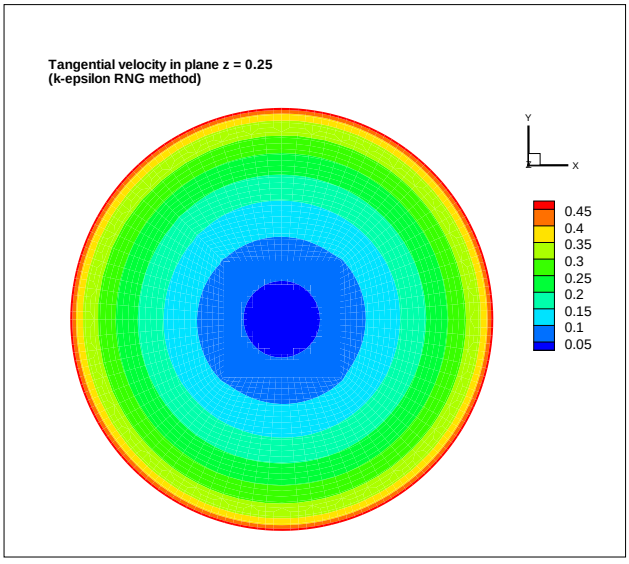


*Figure 4.2 Actual tangential velocity in the plane z = 0.25. (cf. fig. 4.8)*

Also shown in figure 4.3 are three streamlines of velocity, spiraling inwards. Note how the streamlines stop suddenly, indicating that the particle exits the plane z = 0.25. According to the contours,

this means they move in a spiraling motion towards the short end of the drum at z = 0.3048. For illustrative purposes, figure 4.4 shows the radial velocities, that is, velocities along the plane towards or away from the center.

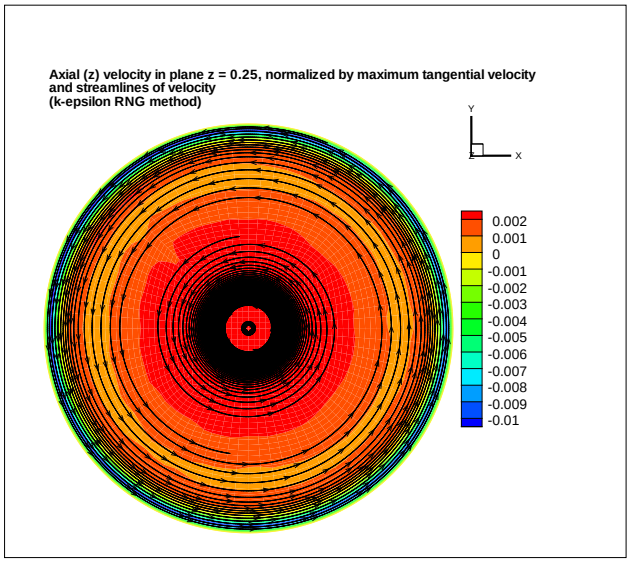


*Figure 4.3 Axial (z) velocity in the plane z = 0.25, normalized by maximum tangential velocity, and velocity streamlines. (cf. fig. 4.8)*

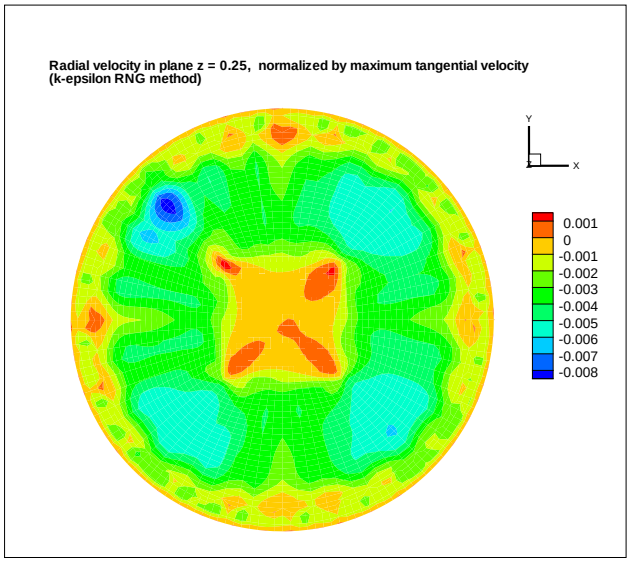


*Figure 4.4 Radial velocity in the plane z = 0.25, normalized by maximum tangential velocity. (cf. fig. 4.8)*

The values of axial and radial velocity are here given as percentages of tangential velocity, so the maximum positive value of axial velocity is 0.3 % of 0.47 m/s (or 0.0014 m/s). Close to the center, where the tangential velocity is closer to zero, the relative axial velocity has larger effect. Being

smaller closer to the walls, the axial velocity is very small compared to the tangential velocity.

The flow would therefore tend to spiral from the center towards one of the circular side walls of the drum, turn to the corners where the stagnation builds up whirls as those shown in figure 4.1. From the outer periphery it would slowly make its way back to the center along the symmetry line. Consider the injection of aerosols at the center. Assuming they follow the flow, the described path is the one they will follow. A 3-D illustration of the flow pattern is given in figure 4.5, which sums up the previous discussion.

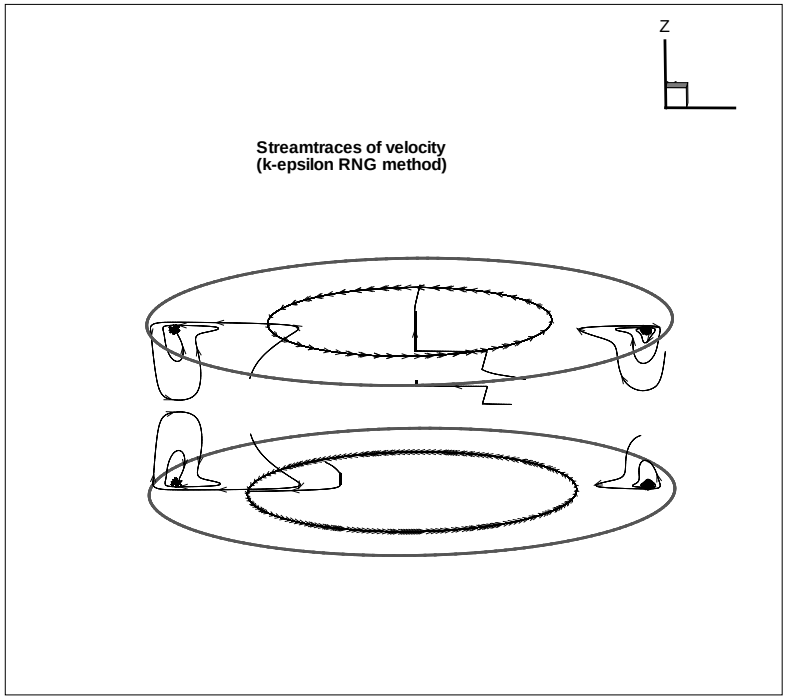


*Figure 4.5 3-D plot of the chamber, showing particle paths.*

To estimate how long time it would take for an aerosol to circulate the camber once, the flow pattern described above is divided into four different motions. The first one is from the center of the chamber to the circular side wall, a distance of 0.3048 $m$. This is approximated to only depend on the axial velocity, which is $0.000958\ m/s$ (cf. fig. 4.3) giving a time of $318\ s$. The second depends on both the radial and tangential velocity and describes the spiraling motion. For each lap around the chamber, the following lap will change with the angle $\alpha$, where $\alpha = \arctan \frac{u_r}{u_t}$. Here, $u_r$ is the radial velocity (approximately $0.0007185\ m/s$) and $u_t$ is the tangential velocity (approximately $0.25\ m/s$). So for each lap there will be a change in angle of $0.1662°$, which correspond to a change in radius of $0.0027\ m$. Hence, an aerosol would spiral $\frac{R}{\Delta r} \approx 339$ laps in the chamber. An average lap is $2.8727\ m$ which gives a total length of 973.85 $m$ and a time of $3895\ s$. The third motion is from the corner of the chamber to the symmetry plane along the periphery, and is also assumed to only depend on the axial velocity. The average velocity in this region is $4.79 \cdot 10^{-4}\ m/s$, which gives a time of $636\ s$. This is followed by the motion back to the center of the chamber. The average velocity along the symmetry line is very slow, approximately

$2.9 \cdot 10^{-6}\ m/s$, and the time it would take for the aerosol to get back to the center of the chamber thus becomes very long, almost $3.2 \cdot 10^{5}\ s$. The total time for an aerosol to circle the chamber once is almost $3.25 \cdot 10^{5}\ s$ or 3.7 days. This estimation assumes that no deposition on the walls will occur nor that the aerosols will agglomerate in the outer part of the chamber.

## 4.2 Comparison of the models

The turbulence models considered are given below.

- $k - \varepsilon$ standard model
- $k - \varepsilon$ standard model with non-equilibrium wall functions
- $k - \varepsilon$ renormalization-group (RNG) model
- $k - \varepsilon$ realizable model
- $k - \varepsilon$ realizable model in a stationary reference frame
- $k - \omega$ standard model
- $k - \omega$ standard model in a stationary reference frame
- $k - \omega$ shear-stress transport (SST) model
- Laminar (turbulence free) model
- Large Eddy Simulation (LES) model

These models were compared by considering the velocity magnitude. The values were taken at five lines of constant x or z-value through the toroid, cf. figures 4.6 and 4.7. For the LES and laminar method, average velocities are given, as it would be of little meaning to compare instantaneous velocities at different times with averages from the other models.

Contour plots of tangential, radial and axial velocity are also considered and taken at the planes $y = 0$ and $z = 0.25$. The planes are depicted in figure 4.8. The velocities are normalized with respect to the maximal tangential velocity of the wall, and so all velocities are given in percentages of this.

Figures 4.9 through 4.15 display the velocity magnitude $|\vec{v}| = \sqrt{\bar{u}^2 + \bar{v}^2 + \bar{w}^2}$ at the different lines for different models. As will be clear later, the radial (u) and axial (w) components will be very small compared to the tangential component (v), which by far will dominate the resulting velocity magnitude.

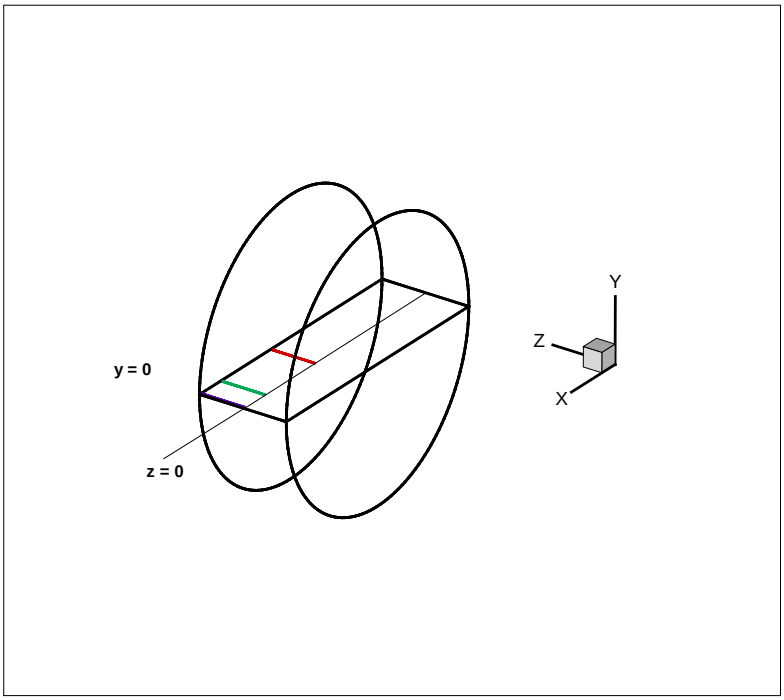


*Figure 4.6 Lines through the toroid at lines of constant x-values, x = 0.2, x = 0.7 and x = 0.9.*

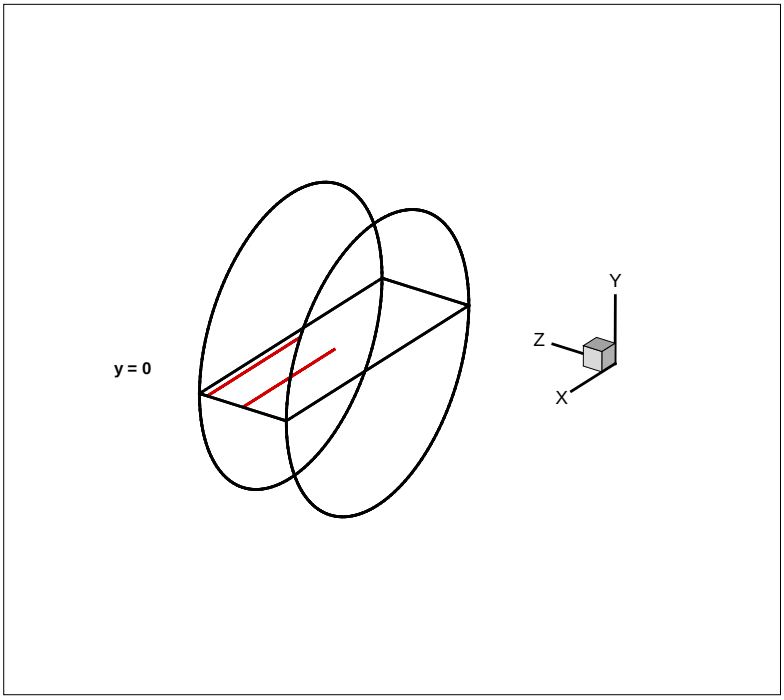


*Figure 4.7 Lines through the toroid at constant z-values, z = 0 and z = 0.25, x from center and out.*

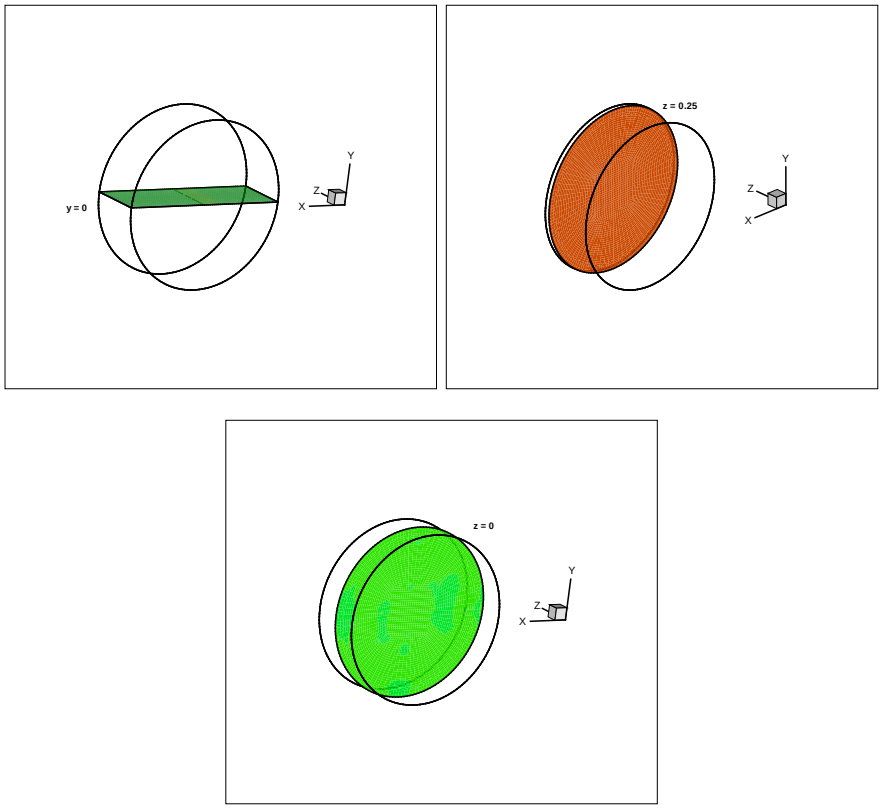


*Figure 4.8 Planes y = 0, z = 0.25 and z = 0 in the rotating drum*

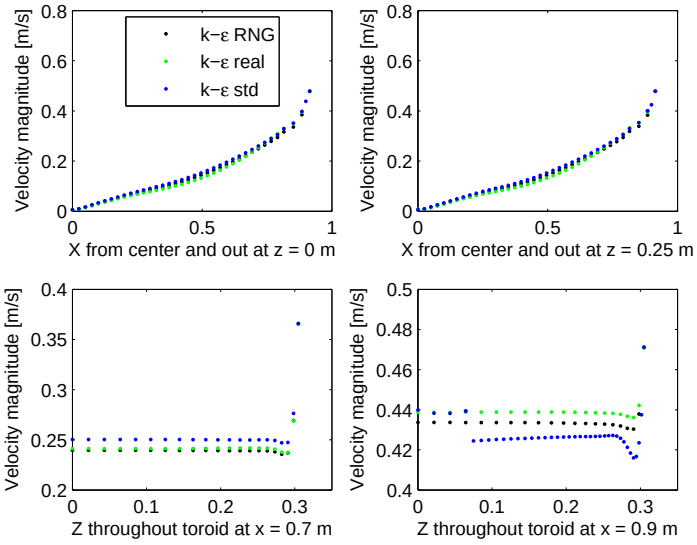


*Figure 4.9 Comparison of the various $k-\varepsilon$ models, at the different lines. (cf. figs. 4.6, 4.7)*

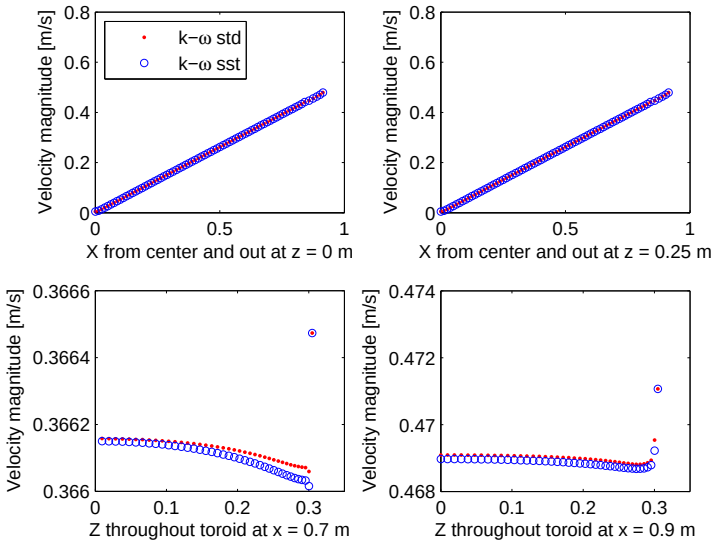


*Figure 4.10 Comparison of the various $k-\omega$ methods, at the different lines. (cf. figs. 4.6, 4.7)*

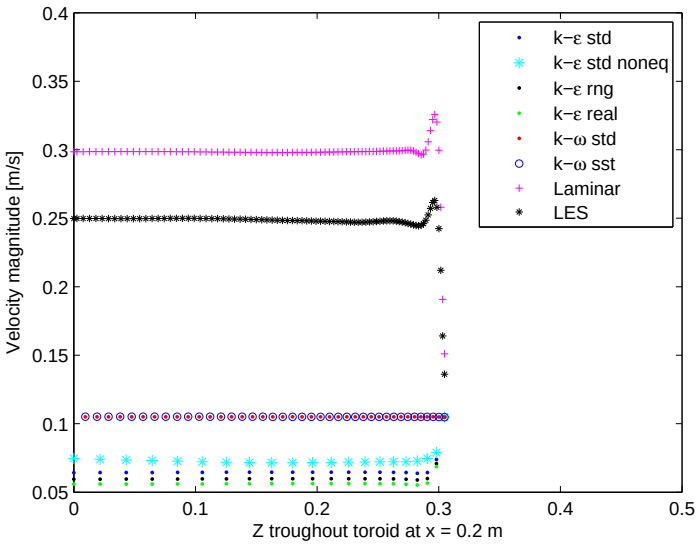


*Figure 4.11 Comparison of all the models, at the inner line x = 0.2 (cf. fig. 4.6)*

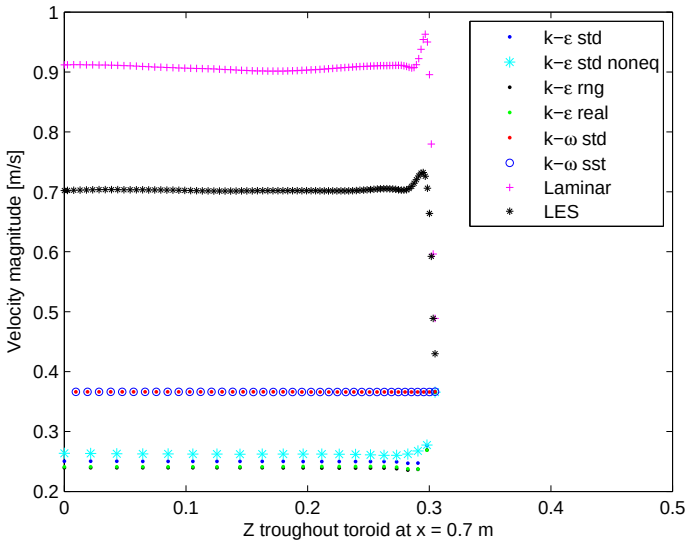


*Figure 4.12 Comparison of all the models, at the middle line x = 0.7 (cf. fig. 4.6)*

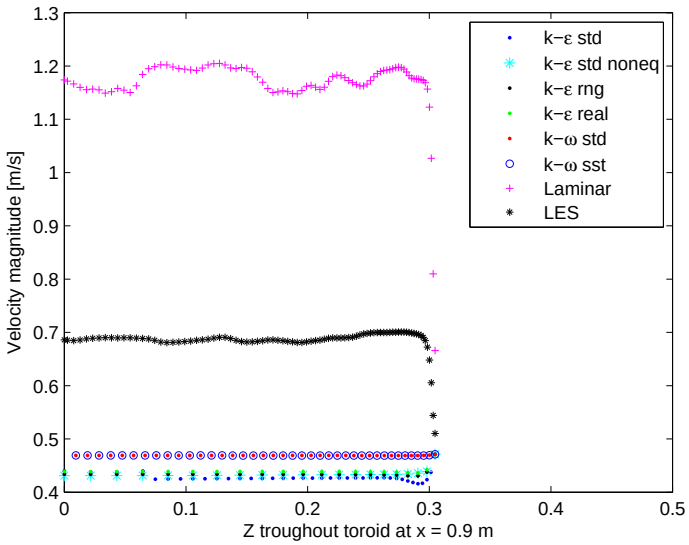


*Figure 4.13 Comparison of all the models, at the outer line x = 0.9 (cf. fig. 4.6)*

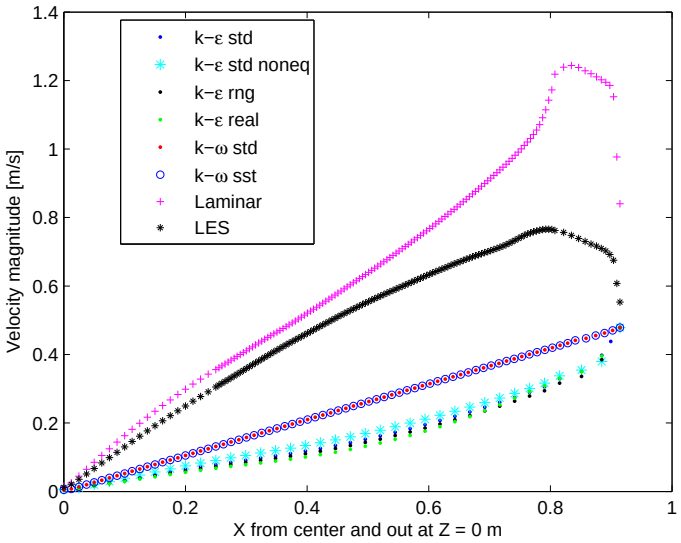


*Figure 4.14 Comparison of all the models, at z = 0 (cf. fig. 4.7)*

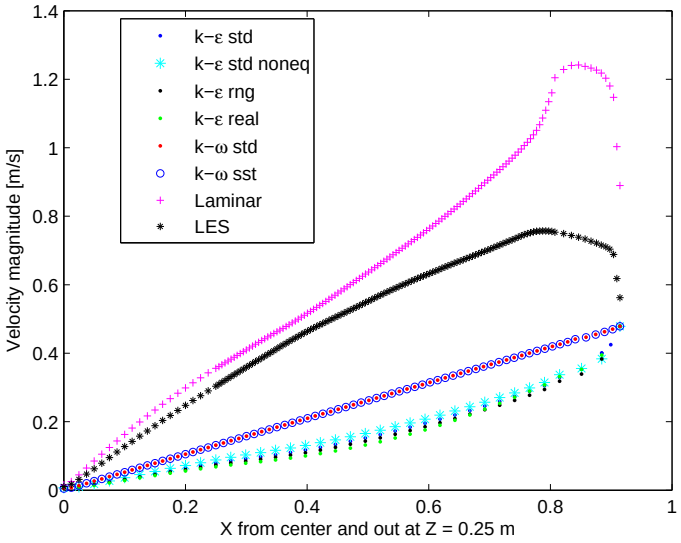


*Figure 4.15 Comparison of all the models, at z = 0.25 (cf. fig. 4.7)*

The $k-\omega$ models show linear velocity profiles, implying a solid body rotation. The velocity profiles given by the $k-\varepsilon$ models show fully developed turbulent flows. We would expect velocity profiles closer to those generated by the $k-\varepsilon$ methods, and the $k-\omega$ models clearly stand out from the rest, both in the line plots and in the contour plots. The obtained results are clearly unphysical and therefore discarded.

The laminar model and the LES generally give larger velocities than the other models. The difference grows as we approach the wall, and then decays, as the laminar and LES curves decrease rapidly. All models give the correct velocity at the wall, naturally, as this is our boundary condition for the rotational speed of 5 rpm. In figure 4.13, the velocities at the line x = 0.9 are plotted (this is the purple line close to the edge in figure 4.6, 1.44 cm from the wall). Here we see a large difference when comparing the laminar model and the LES to the RANS models. The tangential velocity even becomes larger than the imposed wall velocity, which we know to equal 0.479 m/s. The laminar model gives velocities up to 1.2 m/s at the line x = 0.9. The LES is slightly better at 0.7 m/s, but this is still too high. These results are also unphysical and therefore discarded. The reason for this is still not known, but there is a laminar-turbulent transition close to the outer wall that makes the flow in this region particularly challenging to model. The grid sensitivity of this can (due to thin Ekman boundary layer along the circular wall) also play an important role.

## 4.3 Viscosity ratio and Reynolds number

The eddy viscosity ratio, $\frac{\mu_t}{\mu}$, is the ratio between the turbulent viscosity and the molecular dynamic viscosity, and gives us an indication of how strong the influence of the turbulence is. Contour plot of this ratio gives an indication about the turbulence in the flow; the larger the ratio, the more turbulent the flow is. If this ratio is less than one, we have laminar flow. Plots of eddy viscosity ratio of selected models are given in figures 4.16 through 4.22. For the laminar model, which does not model turbulence, a plot of cell Reynolds number is given instead. The Reynolds number measures the ratio of inertial forces to viscous forces, and so also gives a measure of turbulence.

As expected, we have the largest value near the walls. This goes for all models except the $k-\omega$ models, again indicating that these models might fail in modelling this problem. They give the maximum in the middle, and the values are also much higher than for the other models. This even though the graphs indicated laminar flow. All this makes it difficult to trust the results given by the $k-\omega$ models.

## 4.4 Comparison of different wall functions

Turbulence is highly affected by walls, and so how one chooses to model the flow in the near-wall region is important. In all models enhanced wall treatment has been applied during the simulation. This is because, in high Reynolds number flows, the use of wall functions as opposed to near-wall

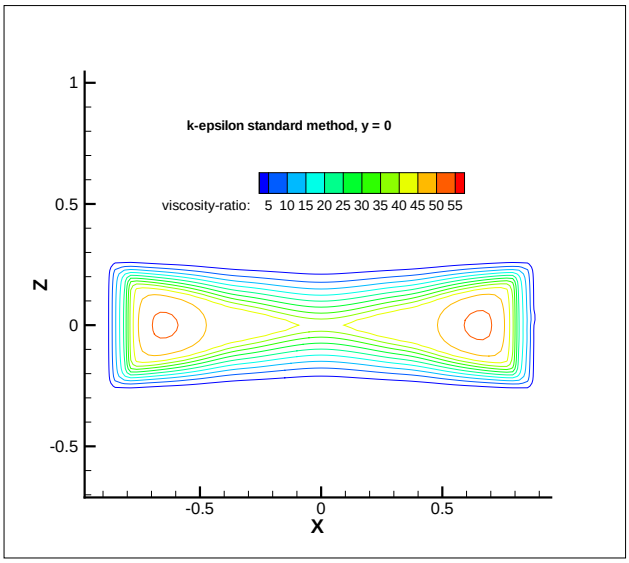


*Figure 4.16 The $k-\varepsilon$ standard method: contours of viscosity ratio. (cf. fig. 4.8)*

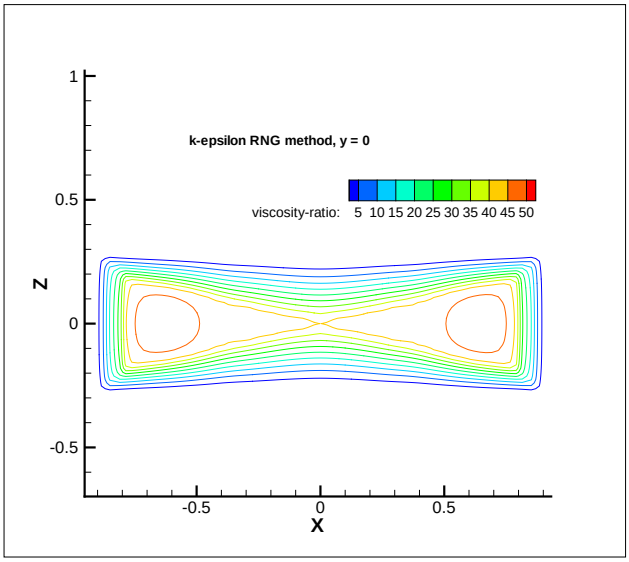


*Figure 4.17 The $k-\varepsilon$ rng method: contours of viscosity ratio. (cf. fig. 4.8)*

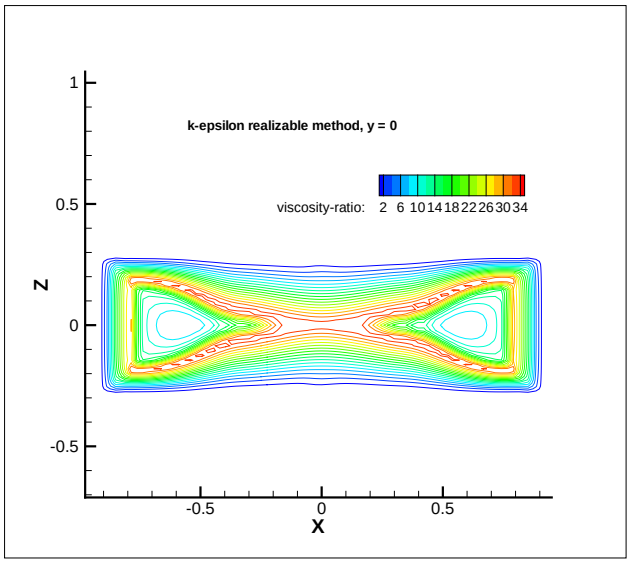


*Figure 4.18 The $k-\varepsilon$ realizable method: contours of viscosity ratio. (cf. fig. 4.8)*

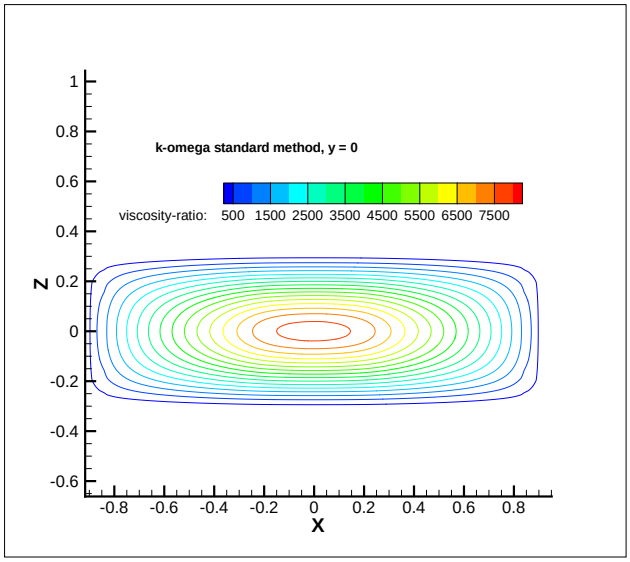


*Figure 4.19 The $k-\omega$ standard method: contours of viscosity ratio. (cf. fig. 4.8)*

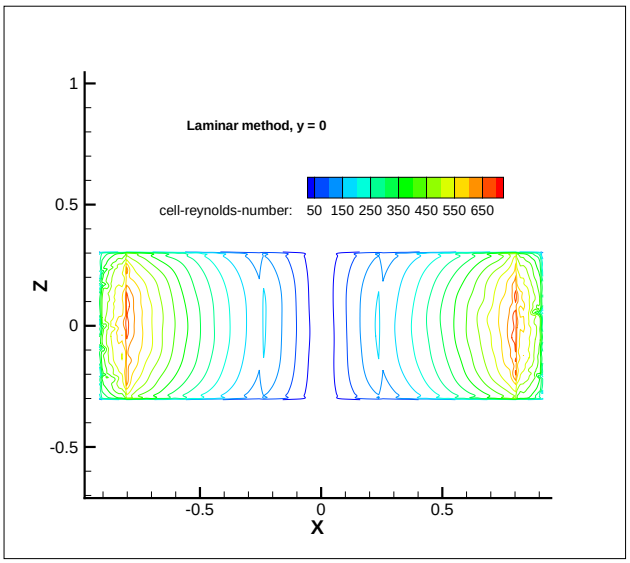


*Figure 4.20 The laminar method: contour plot of Reynolds number in the plane y = 0, giving an indication of the existence of turbulence. (cf. fig. 4.8)*

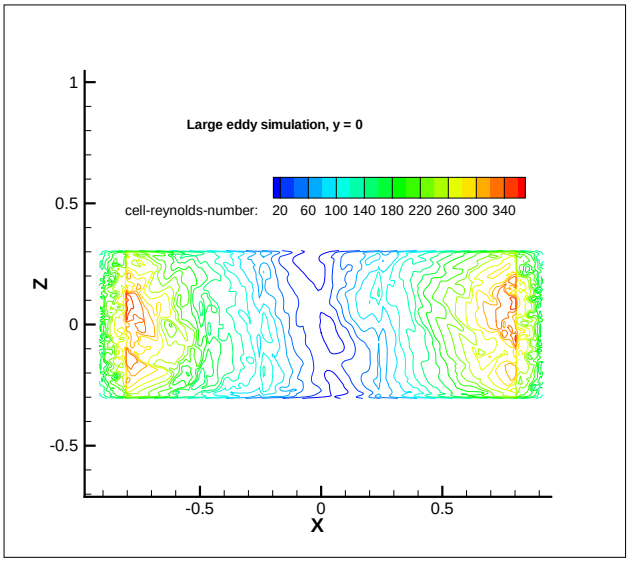


*Figure 4.21 The LES method: contour plot of Reynolds number in the plane y = 0, giving an indication of the existence of turbulence. (cf. fig. 4.8)*

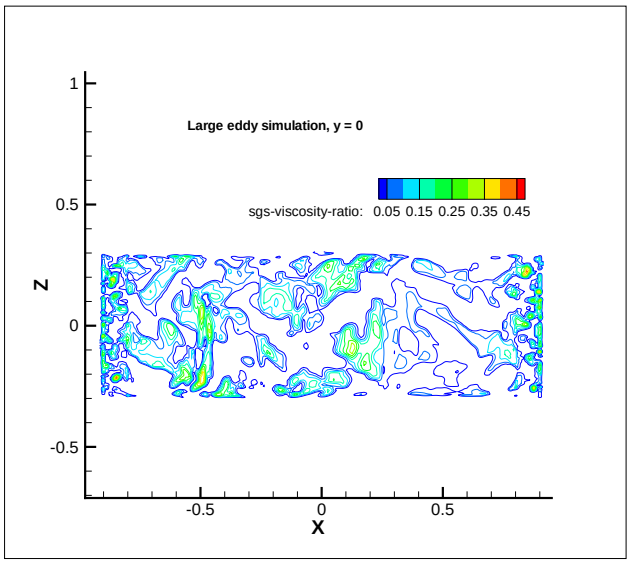


*Figure 4.22 The LES method: contours of subgrid viscosity ratio. (cf. fig. 4.8)*

modelling saves computational time. We have seen that the most of the turbulence resides close to the walls, so this is the region where the solution variables change most rapidly.

As walls are the only thing affecting our computational domain, and hence the flow, we would like to see how the choice of wall function affects the solution. To this end, the $k - \varepsilon$ method was simulated again with the same parameters, applying non-equilibrium wall functions. Non-equilibrium wall functions are recommended for use in complex flows with high pressure gradients, while enhanced wall treatment combines a two-layer model with enhanced wall functions. Details on the different wall treatments are beyond the scope of this paper, but are given in the Fluent user's guide.

The difference is illustrated in 4.23, and as we see, it is not that large. The effect of applying various wall treatments is of course most apparent in the proximity of the wall. It seems the rotating sidewall of the drum has a larger effect here, judging from the plot at the line x = 0.9. At $z \approx 0.3$, the enhanced wall treatment gives a slightly lower velocity, than do the non-equilibrium wall functions.

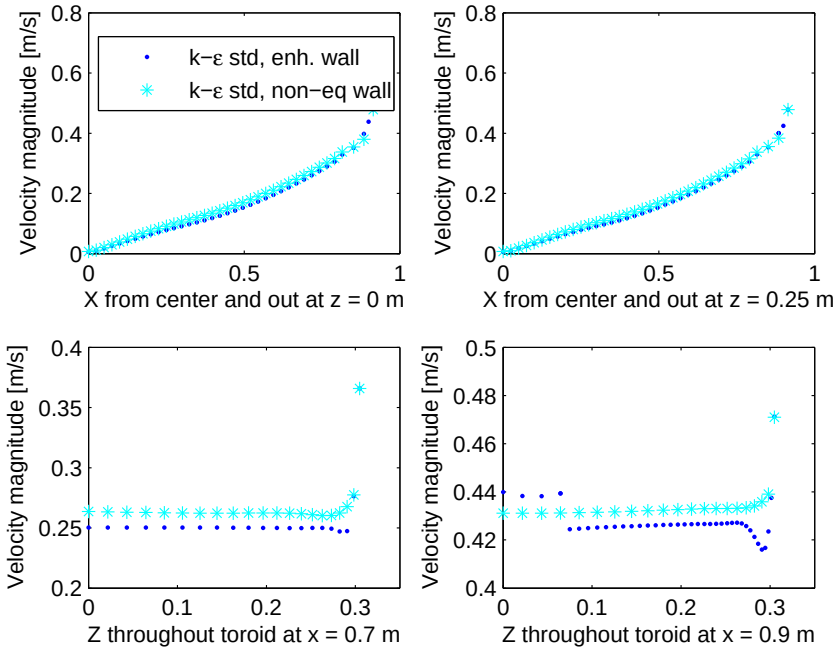


*Figure 4.23 Comparison of the enhanced wall treatment to the non-equilibrium wall treatment, using the $k-\varepsilon$ standard method. (cf. figs. 4.6, 4.7)*

## 4.5 Stationary vs moving reference frame

As mentioned previously, the simplicity of the geometry allows us to view the drum in a single rotating reference frame. We could instead choose to view it in a stationary reference frame, so that the walls would be rotating relative to the interior. Physically, this should make no difference at all. An interesting comparison can be made by simulating the problem in both reference frames.

The $k-\varepsilon$ realizable model is known to not be frame invariant, so we would expect a difference here. To check, we also run the standard $k-\omega$ model in the stationary frame. We then set the interior at rest, while the walls are rotating relatively to it with speed 0.479 m/s, as mentioned in section 6. The results for the $k-\varepsilon$ realizable model are given in figure 4.24. There clearly is a difference, verifying that the model is not frame invariant.

For the standard $k-\omega$ model we expected equal results in the two frames. However, as seen in figure 4.25, this is not the case. In fact, the difference is even larger than it was for the $k-\varepsilon$ realizable model. Why this is, remains a mystery.

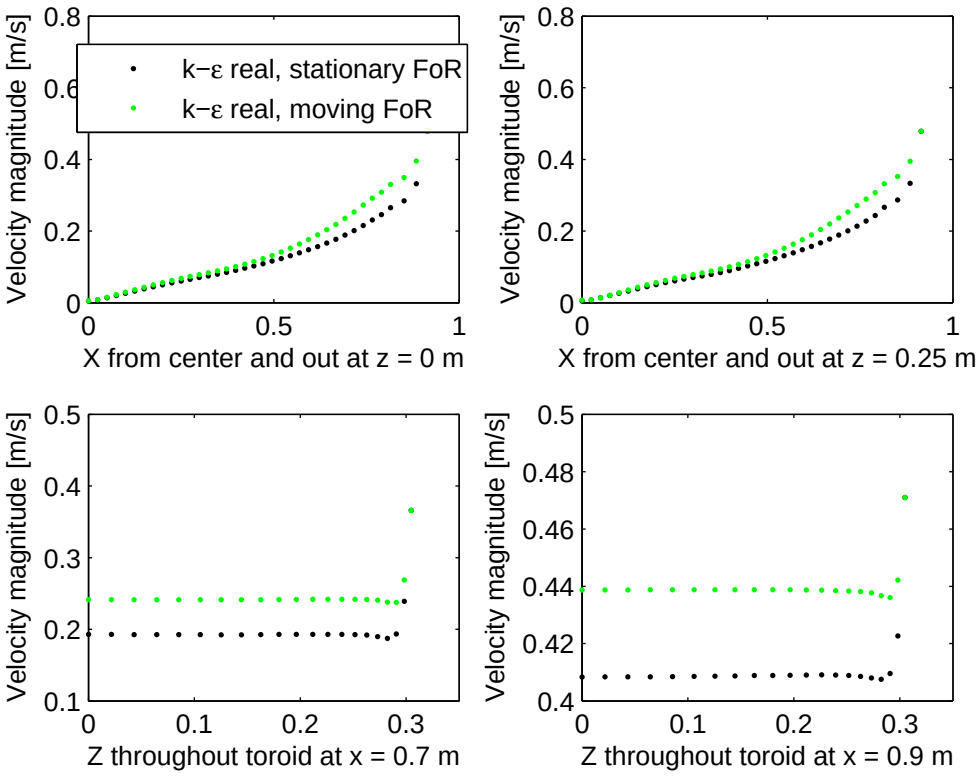


*Figure 4.24 $k-\varepsilon$ realizable method, moving interior vs. moving walls. (cf. figs. 4.6, 4.7)*

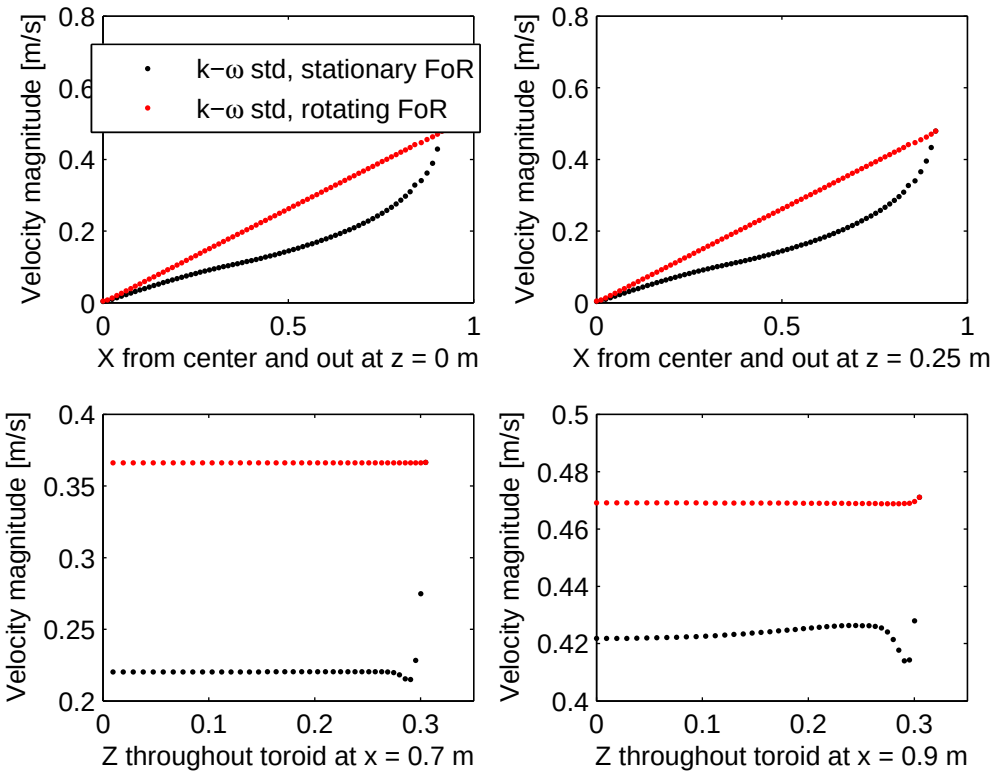


*Figure 4.25 $k-\omega$ standard method, moving interior vs. moving walls. (cf. figs. 4.6, 4.7)*

# 5 Conclusions and further work

The general flow pattern within a rotating aerosol chamber has been studied. Assuming particles that have similar physical properties to that of air, they will follow the flow without affecting it. After being injected into the center, the particles will then slowly move axially towards the circular sidewall of the chamber. In addition they will rotate in the tangential direction. When the particles get close to the sidewall, they will rotate in larger and larger tangential circles, which makes them convect radially towards the peripheral outer wall. As the outer wall is approached, the particles will move towards the plane of symmetry z = 0, before spiraling back towards the place of injection, the center of the chamber. This is the general flow pattern within the chamber, particles might deposit on the wall if they get too close.

The small magnitude of the recirculating velocity field predicted in this study is fully consistent with the experimental finding that aerosols may be airborne for very long time. A rough estimate gives that the time it takes for a particle to circulate the chamber once is in order of hours.

Different RANS models as well as a laminar model and an LES have been compared. The models gave quite different results, and some might not be suitable for these kind of problems.

In this study, the rotational speed has been 5 rpm, consistent with the highest of the three used in (2). However, in the article by Gruel et. al. (4), the optimum rate of rotation is investigated, and found to be varying from 0.29 to 1.41 rpm, which is much lower than previously used. They find the optimum rotation rate to be dependant of the radius of the drum and the particle sizes, however, for particles of diameters up to 10 $\mu m$, the optimum rate is claimed to be independent of the particle sizes. The effect of slowing down the drum should be investigated further.

To inject the particles, Goldberg et. al. (2) mounted a thin pipe trough the center of the side plane going into the center of the drum. This pipe is not included in the modelling in this study, but will undoubtedly affect the flow in some way, as we no longer have the symmetry.

Upon entering the drum, the particles will inevitably have some velocity, which also will affect their path. This has not been included here, as the main objective has been modelling the general flow within the chamber.

## References


[1] L. J. Goldberg, “Naval biomedical research laboratory, programmed environment, aerosol facility,” 1970.

[2] H. M. S. W. L. J. Goldberg, E. E. Boerke, and M. A. Chatigny, “The use of a rotating drum for the study of aerosols over extended periods of time,” 1956.

[3] *Fluent 6.3 User’s guide*, 6th ed. Fluent Inc., 2006.

[4] C. R. R. R. L. Gruel and R. T. Allemann, “The optimum rate of drum rotation for aerosol aging,” 1986.